Electronic Supplementary Information for

Nitrogen-doping and titanium vacancies synergistically promote CO_2 fixation in seawater

Di Qu et.al.

Experimental Section

Synthesis of NTC-V_{Ti}

For the preparation of the NTC-VTi catalyst, Ti_3C_2 Mxene was firstly synthesized according to our previously reported work (*J. Mater. Chem. A* 2020, 8, 8913–8919). Subsequently, 50 mg the prepared Ti_3C_2 Mxene sample was annealed under an NH3 atmosphere in a quartz pipe furnace at 500 °C for 2 h with a heating rate of 5 °C min^{-1} to obtain the NTC-V_{Ti} sample.

Characterizations

XRD patterns were performed by an X-ray diffractometer (SmartLab 9kW) at a scan rate of 1° min^{-1} from 5 to 70°. The N_2-sorption isotherms and pore size distribution curves for the $(VO)_2P_2O_7$ nanosheets were obtained by the Brunauer–Emmett–Teller (BET) measurement with an Autosorb-iQ-MP Micromeritics analyzer. The field-emission-gun SEM instruments (Quanta FEG 250 and Verios 460L of FEI) were applied in the SEM characterization. TEM and EDS images were achieved via TEM instruments, namely JEOL JEM-2100 and FEI Talos F200X. XPS results were recorded by a Kratos AXIS Ultra DLD system with the Al Kα radiation as the X-ray source. Meanwhile, the C 1s peak has been fixed at the binding energy of 284.8 eV.

Electrochemical measurements

All the electrochemical experiments were performed in a gas-tight H-cell separated by a Nafion N117 membrane using an electrochemistry workstation (CHI760E Shanghai Chenhua Instrument Co.). The working electrodes were catalysts-coated carbon paper (1 x 1 cm) with a loading of 0.2 mg cm^{-2}. The Ag/AgCl (saturated with KCl) and graphite rod were used as the reference electrode and counter electrode, respectively. The electrochemical experiments were carried out in seawater at room temperature (25 °C) and under atmospheric pressure. Before every experiment, the electrolyte of the cathodic compartment of the cell was purged with CO_2 (99.99%) for 10 min to obtain a CO_2-saturated solution. During the electrolysis, CO_2 was continuously bubbled into the catholyte with a flow rate of 20 sccm. LSV curves were performed at a sweep rate of 10 mV s^{-1}. Electrochemical impedance spectroscopy (EIS)

measurements were performed using the CHI 760E electrochemical workstation in seawater under an open-circuit potential in the frequency range from 10^{-1} to 10^{5} Hz with an alternating current (AC) voltage amplitude of 5 mV. All initial data has been corrected by *i*R compensation, and the potential value was calculated according to the following equation:

$$E_{RHE} = E_{Ag/AgCl} + 0.0591 \times pH + 0.197$$

In the test, the concentration of gaseous samples was measured using on-line gas chromatography (GC, 7890B Agilent) equipped with a flame ionization detector (FID) and a thermal conductivity detector (TCD). The liquid products were analyzed through ^{1}H spectrum using a nuclear magnetic resonance (NMR, AVANCE AV III 400 Bruker) equipment, and DMSO was used as an internal standard for quantification. In the work, no liquid product can be detected.

The Faradaic efficiency (FE) of CO can be calculated by the following equation:

$$FE= (2nC \times V_{CO2} \times 10^{-3} \times t \times F)/22.4Q$$

where n is the exchanged electron numbers to CO, C is the volume concentration of the gas products, measured by gas chromatography; V_{CO2} is the CO_2 flow rate; t is electrolysis time; F is the Faradaic constant (96485 C mol^{-1}); Q is the amount of cumulative charge during the CO_2 reduction reaction.

Computational details

Density functional theory (DFT) calculations were performed using the DMol^3 code. The Perdew, Burke and Ernzerhof (PBE) exchange-correlation functional within a generalized gradient approximation (GGA) was employed as an exchange-correlation functional. The basis functions were the double numerical plus polarization (DNP) set. The *k*-point sampling of the Brillioun zone was done using a 5 × 5 × 1 grid for geometry optimizations.

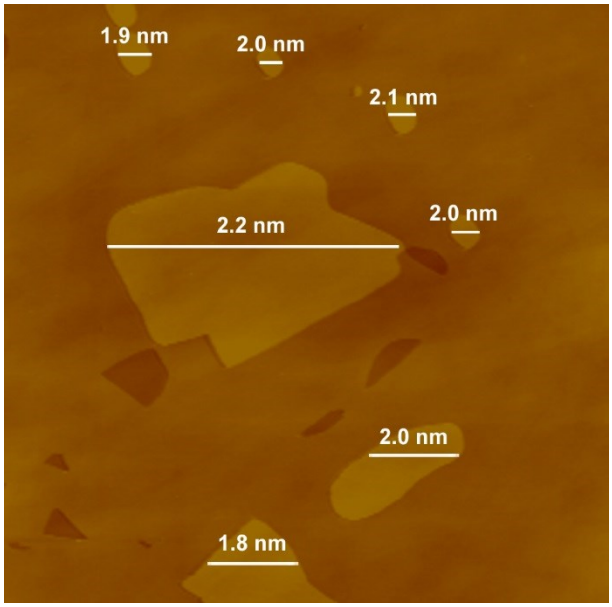

Figure S1. AFM image and the corresponding hight profiles of NTC-V_{Ti}.

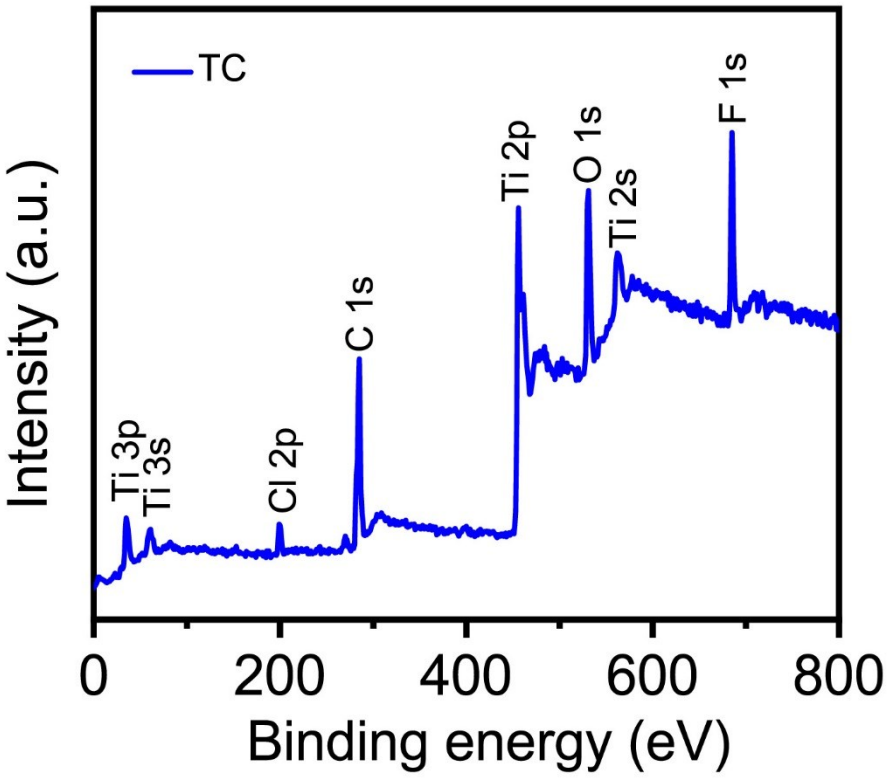

Figure S2. XPS survey spectrum of TC.

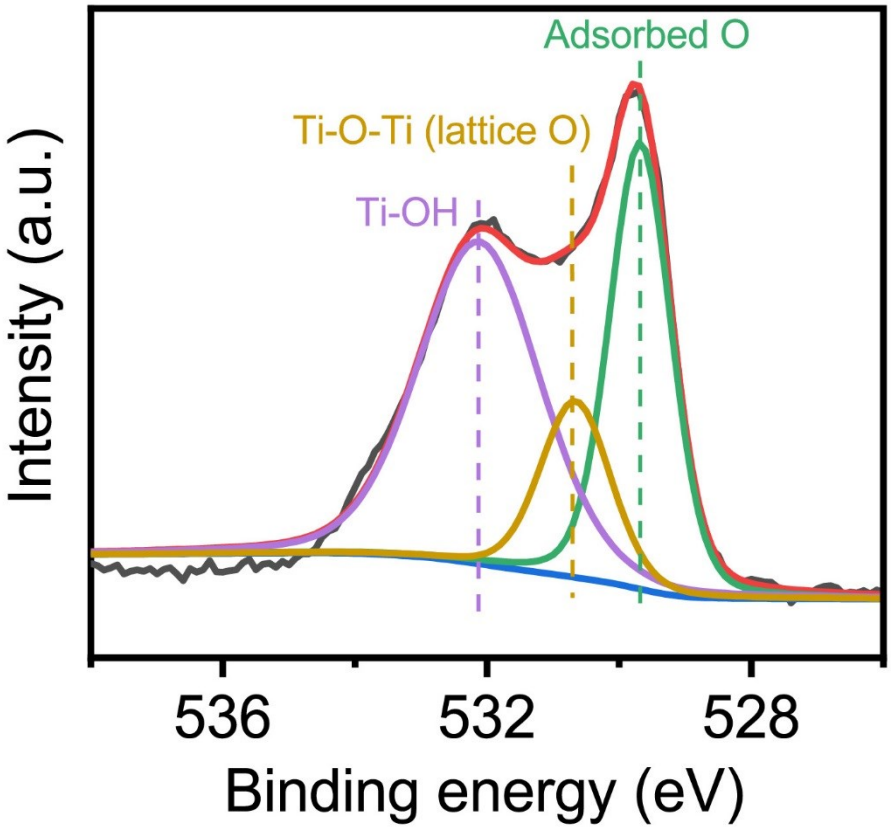

Figure S3. High-resolution XPS spectrum for O 1s of NTC-V_{Ti}.

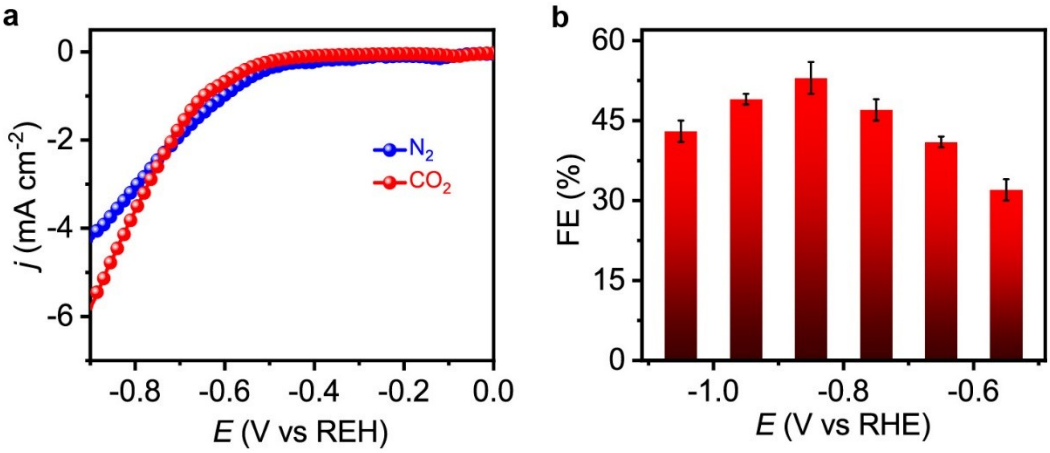

Figure S4. CO_2RR performance of NTC-V_{Ti} tested in 0.5 M $KHCO_3$. (a) Polarization curves of NTC-V_{Ti} recorded in N_2- and CO_2-saturated 0.5 M $KHCO_3$. (b) FE_{CO} at different applied potentials.

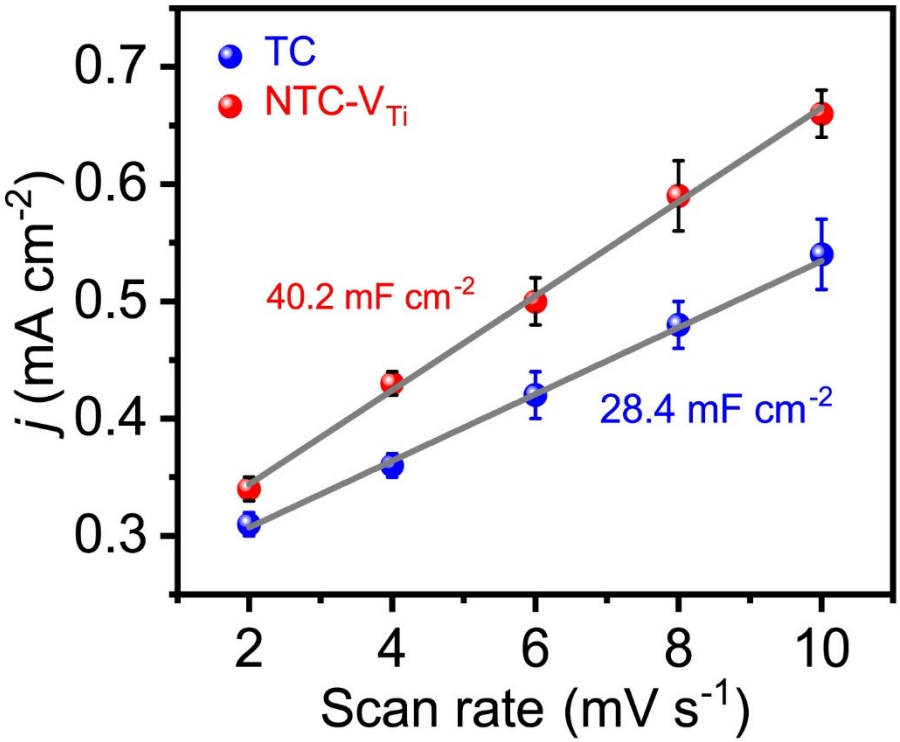

Figure S5. Charging current density differences plotted against scan rates.

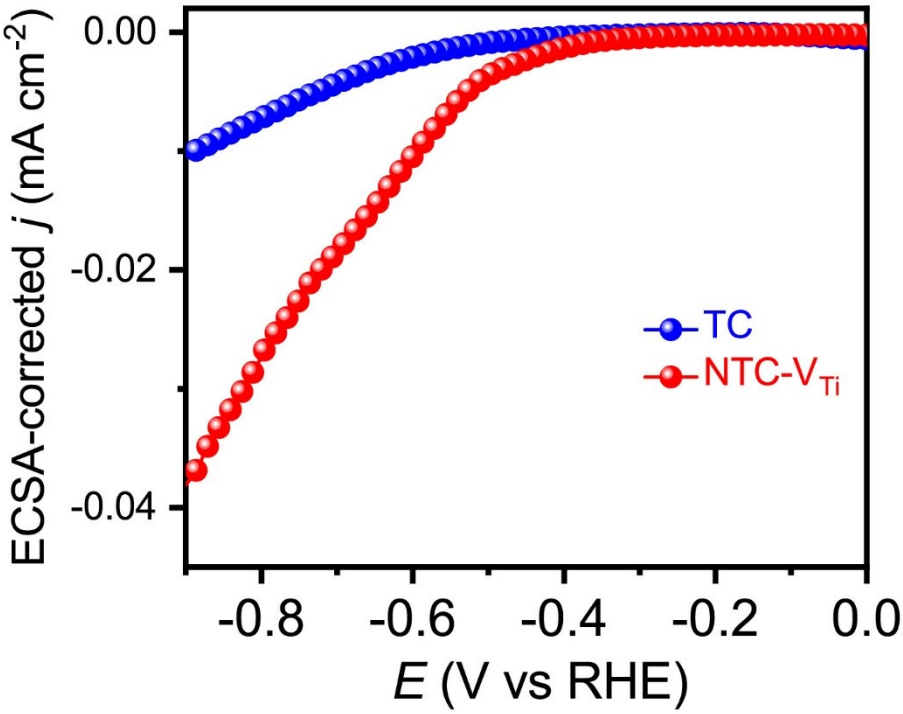

Figure S6. ECSA-corrected current densities versus applied potentials.

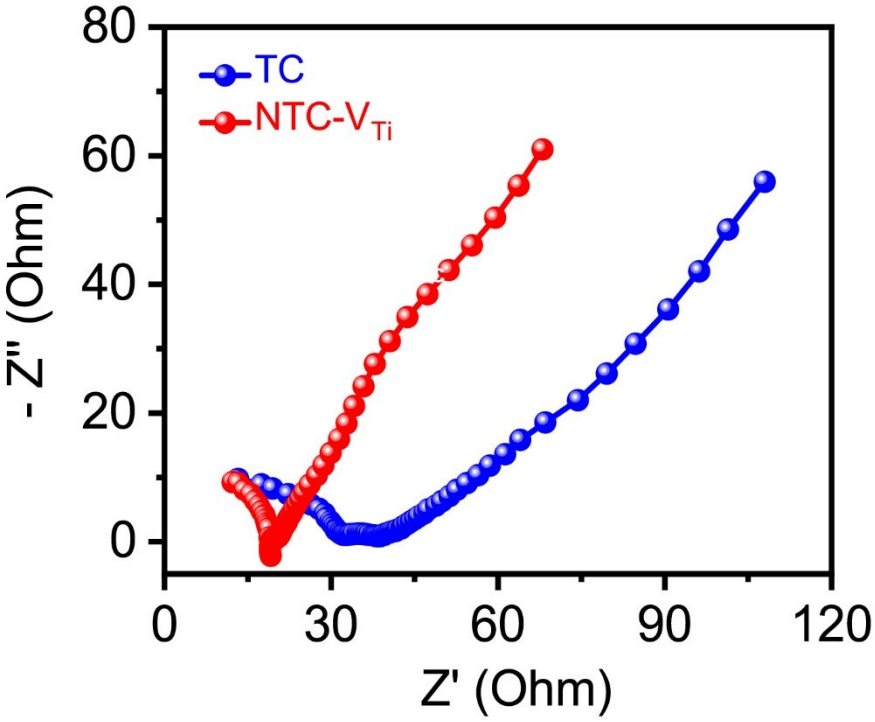

Figure S7. EIS spectra of NTC-V_{Ti} and TC.

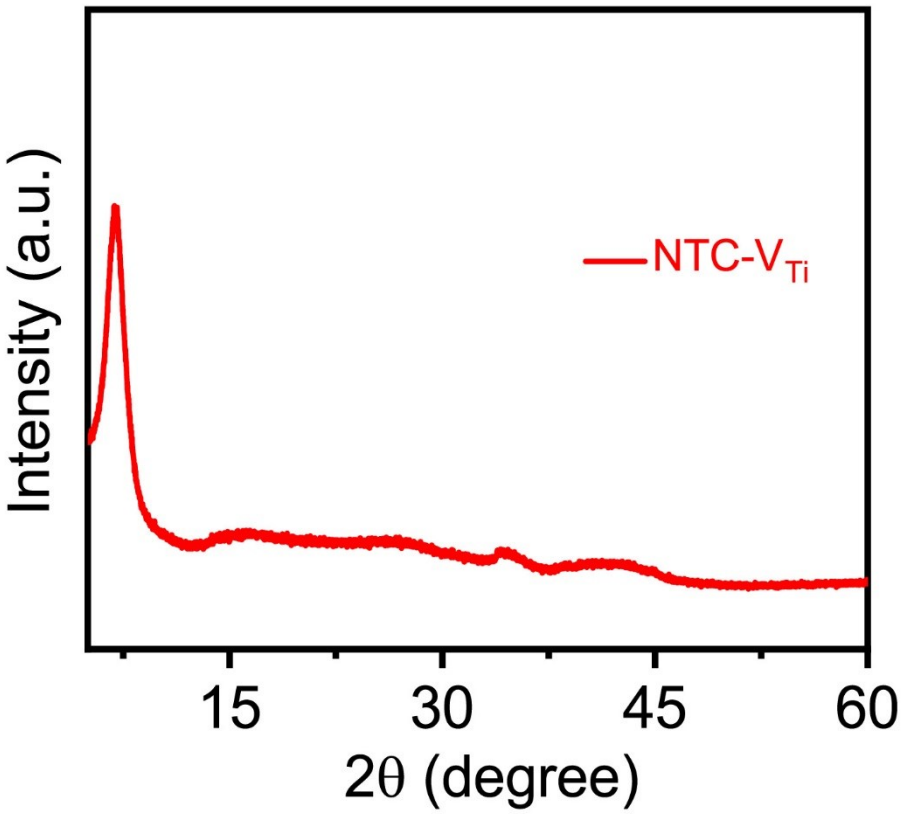

Figure S8. XRD pattern of NTC-V_{Ti} recorded after the long-term electrolysis.

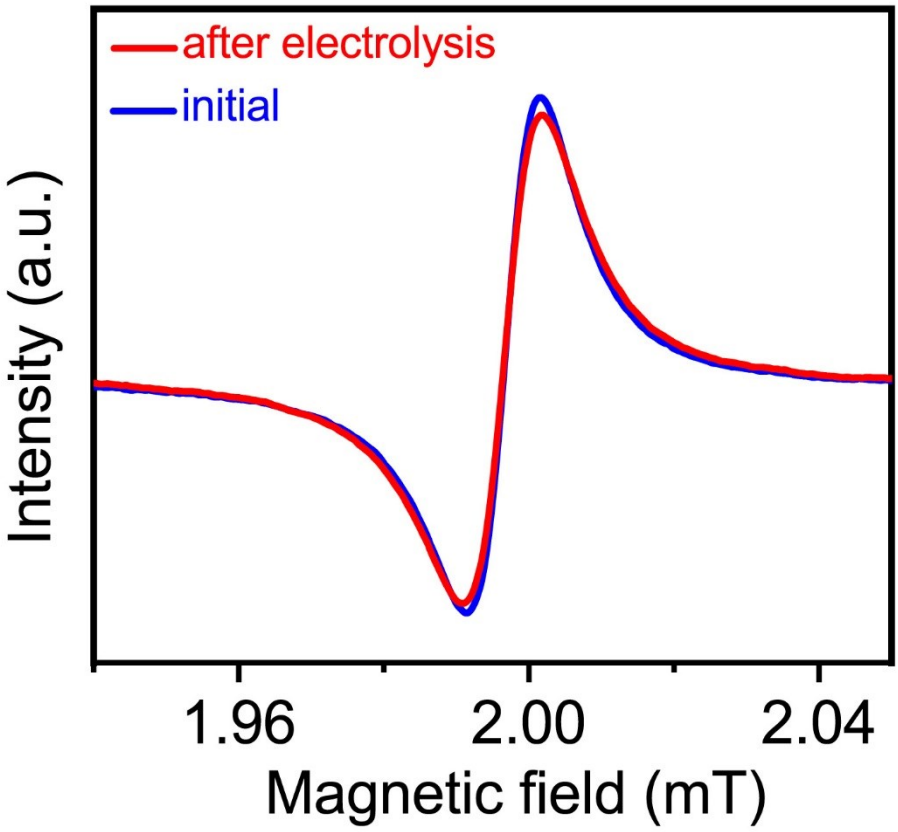

Figure S9. EPR spectrum of NTC-V_{Ti} taken after the long-term electrolysis.

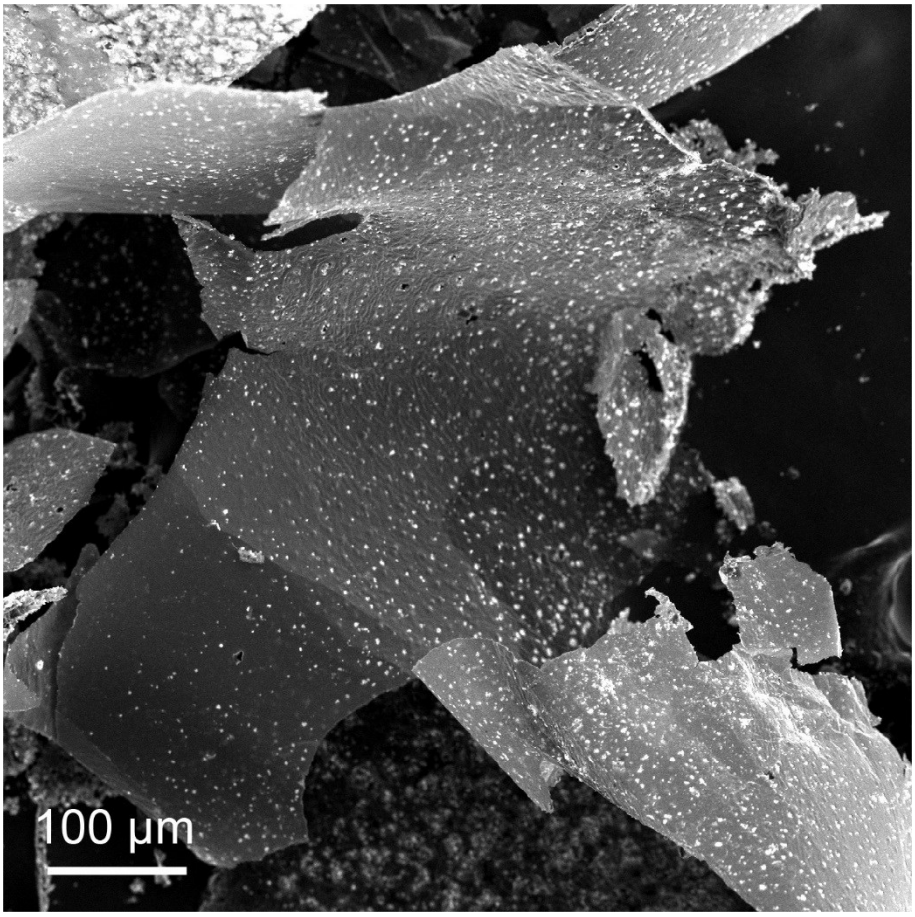

Figure S10. SEM image of NTC-V_{Ti} taken after the long-term electrolysis.

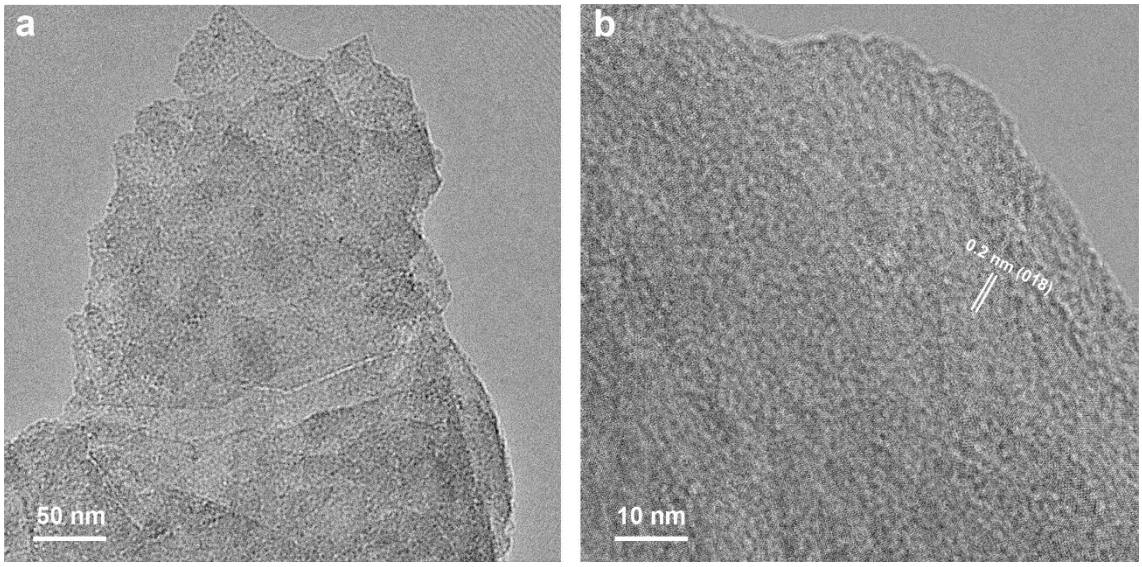

Figure S11. TEM and HRTEM images of NTC-V_{Ti} taken after the long-term electrolysis. The HRTEM image presents characteristic lattice spacing of 0.2 nm, which can be ascribed to the (018) plane of Ti_3C_2 MXene.

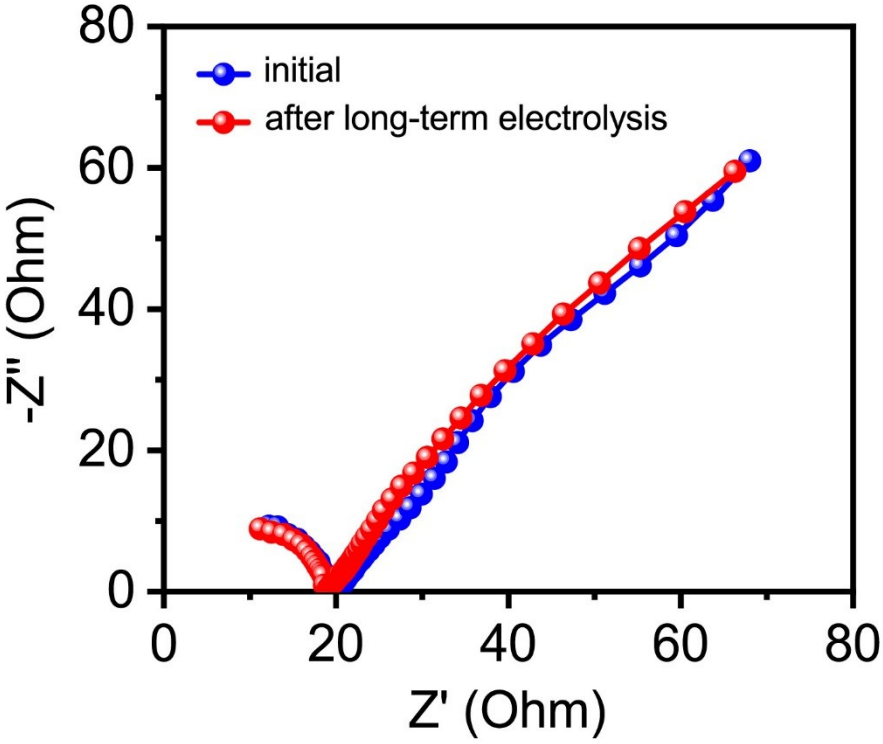

Figure S12. EIS spectra of NTC-V_{Ti} taken before and after the long-term electrolysis. Note that the black pattern is the same as the red one in Figure S7.

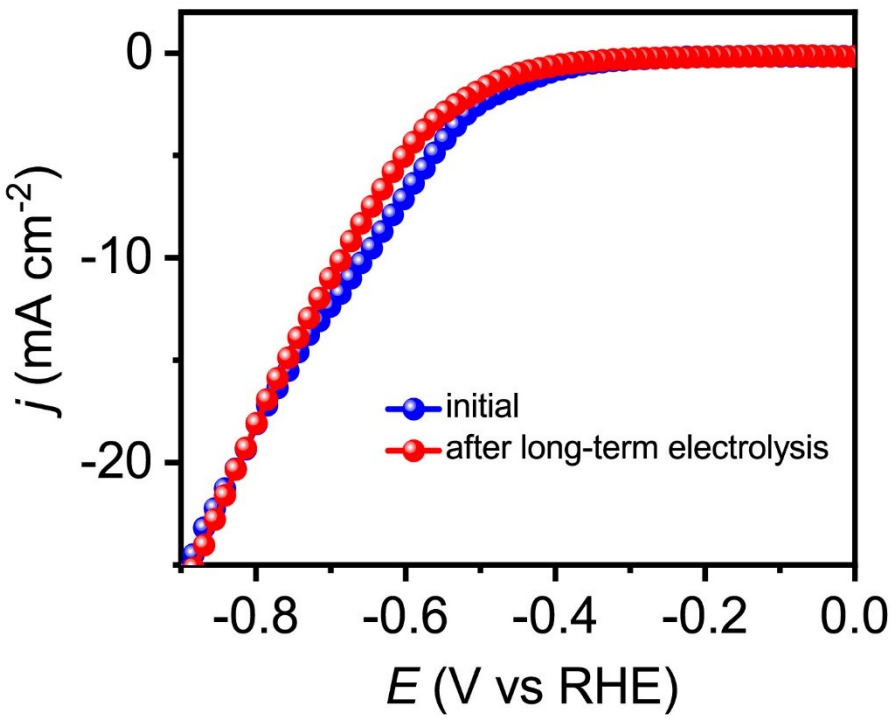

Figure S13. CO_2RR polarization curves of NTC-V_{Ti} taken before and after the long-term electrolysis. Note that the blue pattern is the same as the red one in Figure 3a.

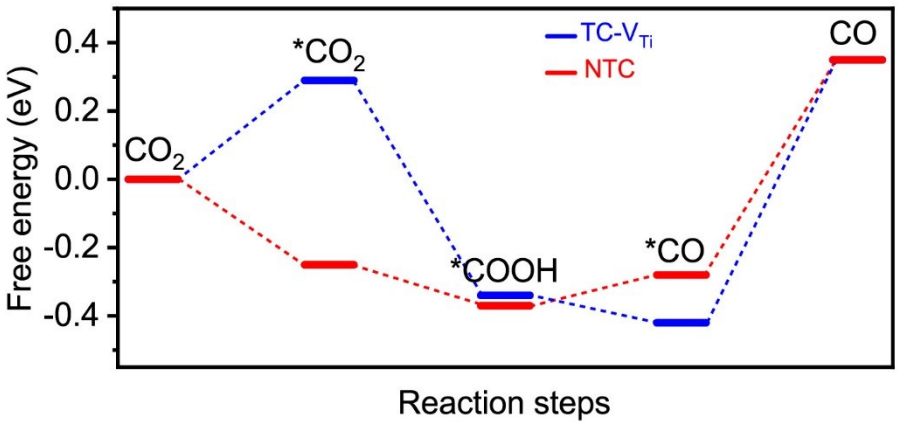

Figure S14. Calculated free energy of CO_2RR on NTC and TC-V_{Ti} surfaces.

Table S1. HER electrocatalysis results of this work and those reported in the literature.

Catalysts	Electrolyte	FE (%)	j_{CO} (mA/cm^2)	Potential (V vs. RHE)	Reference
			Noble metal-based catalysts		
Au/Py-CNTs-O	0.1 M $KHCO_3$	93	~6.51	−0.58	*ChemSusChem* ***2019****, 12, 1724*
Pd{3 1 0}	0.1 M $KHCO_3$	90.6	~4.53	–0.9	*Chem. Eng. Sci.* ***2019****, 194, 2, 29*
Pd-Ag	0.5 M $KHCO_3$	97.3	2.85	–0.7	*ACS Sustain. Chem. Eng.* ***2019****, 7, 3536*
Pd nanosheets	0.1 M $KHCO_3$	94	~2.82	–0.5	*Angew. Chem. Int. Ed.* ***2018****, 57, 11544*
Cu-Ag	0.5 M $KHCO_3$	95.7	9.5	–0.8	*ACS Appl. Mater. Interfaces* ***2018****, 10, 43650*
Au/Cu nanoparticles	0.1 M $KHCO_3$	~94	~3.29	–0.8	*J. Phys. Chem. C* ***2018****, 122, 27991*
Au-CeOx/C	0.1 M $KHCO_3$	89.1	12.9	–0.89	*J. Am. Chem. Soc.* ***2017****, 139, 5652*
Triangular Ag nanoplates	0.1 M $KHCO_3$	96.8	~1.94	–0.86	*J. Am. Chem. Soc.* ***2017****, 139, 2160*
Oxygen plasma-treated Ag	0.1M $KHCO_3$	90	–	–0.6	*Angew. Chem. Int. Ed.* ***2017****, 56, 11394*
Pd icosahedra/C	0.1 M $KHCO_3$	91.1	~1.82	–0.8	*Angew. Chem. Int. Ed.* ***2017****, 56, 3594*
Oxide-derived Ag	0.1 M $KHCO_3$	89	1.02	–0.6	*Angew. Chem. Int. Ed.* ***2016****, 55, 9748*
Ag-IO	0.1 M $KHCO_3$	80	~29.6	–0.8	*Angew. Chem.* ***2016****, 128, 15508*
3.7 nm Pd nanoparticles	0.1 M $KHCO_3$	91.2	~8.20	–0.89	*J. Am. Chem. Soc.* ***2015****, 137, 4288*
Ultrathin Au nanowires	0.5 M $KHCO_3$	94	8.16	–0.35	*J. Am. Chem. Soc.* ***2014****, 136, 16132*
Ag foam	0.5 M $KHCO_3$	99.5	0.02	–0.3	*ACS Catal.* ***2018****, 8, 8357*
Au-2D	0.1 M $KHCO_3$	87.4	2.4	–0.5	*Nano Lett.* ***2019****, 19, 9154*
Ag_{DP8h}	0.1 M $NaHCO_{3aq}$	98.5	4.4	–0.5	*ACS Sustainable Chem. Eng.* ***2019****, 7, 6352*
Au/C_3N_4	0.5 M $KHCO_3$	90	2.56	–0.45	*ACS Catal.* ***2018****, 8, 11035*
Ag@$AgCl_x$ CSNW	0.5 M $KHCO_3$	90	1.79	–0.46	*ACS Appl. Energy Mater.* ***2019****, 2, 6163*
Nanoporous Ag	seawater	~93 (less than 3h)		–1.2 (vs	*J. Mater. Chem. A,* ***2018****, 6, 23301*

				Ag/AgCl)	
Non-noble metal-based catalysts					
NTC-V_{Ti}	seawater	92 (40 h kept 100%)	~16.2	–0.7	***This work***
DHPC	seawater	~92% (10 h kept 68%)	–	–0.7	*J. Mater. Chem. A* ***2020****, 8, 1205*
Fe^{3+}-N-C	0.5 M$KHCO_3$	90	94	–0.45	*Science* ***2019****, 364, 1091*
Cu-In	0.1 M $KHCO_3$	91	4.1	−0.95	*Electrochim. Acta,* ***2019****, 295, 584*
In_2Se_3 nanosheets	0.1 M $KHCO_3$	89	~15.4	–0.7	*Electrochem. Commun.* ***2019****, 103, 127*
Zn P-NS	0.1 M $KHCO_3$	90	~6.75	–1.0	*Adv. Energy Mater.* ***2019****, 1900276*
MnO_2	0.1 M $KHCO_3$	71	~12	–0.95	*Inorg. Chem.* ***2019****, 58, 8910*
Hexagonal Zn	0.5 M $KHCO_3$	85.4	–	−0.95	*Angew. Chem., Int. Ed.* ***2016****, 55, 9297*
Cu fibers	0.3 M $KHCO_3$	75	~9	−0.40	*Nat. Commun.* ***2016****, 7, 10748.*
Cu–In alloy	0.1 M $KHCO_3$	85	~0.64	–0.60	*Angew. Chem., Int. Ed.* ***2015****, 54, 2146.*
Zn dendrite	0.5 M $NaHCO_3$	79	–	–1.1	*ACS Catal.* ***2015****, 5, 4586*
Fe-CNPs	1.0 M $KHCO_3$	98.8	–	−0.58	*ACS Catal.* ***2019****, 9, 11579*
Ni−N−AC	0.1 M $KHCO_3$	94.8	3.0	–0.8	*J. Phys. Chem. C* ***2020****, 124, 1369*